

Characterization of radial turbulent fluxes in the Santander linear plasma machine

J. A. Mier, R. Sánchez, D. E. Newman, O. F. Castellanos, E. Anabitarte, J. M. Senties, and B. Ph. van Milligen

Citation: *Physics of Plasmas* (1994-present) **21**, 052303 (2014); doi: 10.1063/1.4875722

View online: <http://dx.doi.org/10.1063/1.4875722>

View Table of Contents: <http://scitation.aip.org/content/aip/journal/pop/21/5?ver=pdfcov>

Published by the [AIP Publishing](#)

Articles you may be interested in

[Modification of tokamak edge plasma turbulence and transport by biasing and resonant helical magnetic field](#)
Rev. Sci. Instrum. **84**, 053504 (2013); 10.1063/1.4805066

[Application of wavelet multiresolution analysis to the study of self-similarity and intermittency of plasma turbulence](#)

Rev. Sci. Instrum. **77**, 083505 (2006); 10.1063/1.2336754

[Additional evidence for the universality of the probability distribution of turbulent fluctuations and fluxes in the scrape-off layer region of fusion plasmas](#)


Phys. Plasmas **12**, 052507 (2005); 10.1063/1.1884615


[On the interpretation of fluctuation and \$E \times B\$ turbulent transport measured by Langmuir probes in fusion plasmas](#)

Rev. Sci. Instrum. **75**, 4293 (2004); 10.1063/1.1787575


[Characterization of the frequency ranges of the plasma edge fluctuation spectra](#)

Phys. Plasmas **6**, 4615 (1999); 10.1063/1.873748

A collection of five pieces of Pfeiffer Vacuum equipment: a red rectangular box, a cylindrical metal component, a white rectangular box with 'boehm' and 'ACP' labels, a red cylindrical component with a metal shaft, and a larger white metal chamber.

 Vacuum Solutions from a Single Source

- Turbopumps
- Backing pumps
- Leak detectors
- Measurement and analysis equipment
- Chambers and components

PFEIFFER  **VACUUM**

Characterization of radial turbulent fluxes in the Santander linear plasma machine

J. A. Mier,^{1,a)} R. Sánchez,² D. E. Newman,³ O. F. Castellanos,⁴ E. Anabitarte,¹ J. M. Senties,¹ and B. Ph. van Milligen⁵

¹Departamento de Física Aplicada, Universidad de Cantabria, 39005 Santander, Spain

²Departamento de Física, Universidad Carlos III de Madrid, 28911 Leganés, Madrid, Spain

³Department of Physics, University of Alaska, Fairbanks, Alaska 99775-5920, USA

⁴Instituto de Hidráulica Ambiental, Universidad de Cantabria, 39005 Santander, Spain

⁵Laboratorio Nacional de Fusión, Asociación EURATOM-CIEMAT, 28040 Madrid, Spain

(Received 21 February 2014; accepted 25 April 2014; published online 8 May 2014)

It is shown that the statistical and correlation properties of the local turbulent flux measured at different radial locations of the cold, weakly ionized plasmas inside the Santander Linear Plasma Machine [Castellanos *et al.*, Plasma Phys. Control. Fusion **47**, 2067 (2005)] are consistent with diffusive-like transport dynamics. This is in contrast to the dynamical behavior inferred from similar measurements taken in hotter, fully ionized tokamak and stellarator edge plasmas, in which long-term correlations and other features characteristic of complex, non-diffusive transport dynamics have been reported in the past. These results may shed some light on a recent controversy regarding the possible universality of the dynamics of turbulent transport in magnetized plasmas. © 2014 AIP Publishing LLC. [<http://dx.doi.org/10.1063/1.4875722>]

I. INTRODUCTION

Many theoretical and experimental studies have been done over the years concerning the nature of turbulent radial transport in fusion plasmas.¹ The majority of these studies have been carried out in tokamak^{2,3} and stellarator⁴ devices, that confine a hot, almost fully ionized plasma. A natural radial point of reference for these studies is determined by the location of either a radial limiter or a magnetic separatrix: the Last Closed Flux Surface or LCFS. Inside of the LCFS, magnetic surfaces are closed. Outside, in the region known as the Scrape-Off Layer or SOL region, magnetic field lines are open and continue until they intersect with the limiter, diverter, or first walls. Investigations of the characteristics of turbulent fluctuations and fluxes have been done extensively in the neighborhood of the LCFS mostly by means of Langmuir probes. Most of these studies have concluded that both turbulent fluctuations and fluxes exhibit properties, such as long-term memory or self-similarity within a certain range of scales, that suggest that some kind of non-diffusive, complex transport dynamics might be at play.^{4–10} Similar studies have also been carried out in other magnetized plasmas, either colder or in the presence of open field lines. The evidence is much less clear in these cases. The Thorello device, a toroidal, rotational-transform-less device with plasmas of a few eVs showed no sign of non-diffusive behavior or long-term temporal correlations. Similarly, the plasma within the NAGDIS-II linear machine,¹¹ with also just a few eVs of temperature, showed no sign of long-term correlations in the power-spectrum or correlation of the fluctuations (although it shows multifractal features). On the other hand, other authors have reported stronger similarities with tokamak

transport at the SOL, as was the case of the PISCES device.¹²

To add to this state of things, a novel and different interpretation has been recently put forward that identifies instead the responsible underlying dynamics as some kind of quasi-deterministic, low-dimensional chaos.^{13,14} The main consequence is then that transport takes place through successive random bursts that, when passing by the probe, leave a Lorentzian print. Their randomness thus excludes the kind of long-term correlations that was reported in the previous hot plasma data. Since this new interpretation first originated from the analysis of data from cold, weakly ionized plasmas from the LAPD-U linear plasma machine¹³ (and a small stellarator,¹⁴ TJ-K, that again confines plasmas of just a few eVs), a reanalysis of previously obtained tokamak/stellarator data was undertaken to test whether it made sense to apply these ideas to hot plasmas.¹⁵ The results of this reanalysis were however consistent with previously published results instead of with the newest interpretation. It was also suggested in that work that the extremely different conditions of the plasmas under study (hot, fully ionized versus cold, weakly ionized), together with the fact that linear machines lack magnetic surfaces, could perhaps be responsible for the differences.

To shed some further light on this matter, we analyze here fluctuation data obtained with Langmuir probes in cold (10–50 eV), partly ionized (<10%) plasmas within the Santander Linear Plasma Machine (SLPM).¹⁶ We employ the same techniques that were previously applied to hot tokamak/stellarator plasmas in order to detect long-term correlations and self-similarities. The results support the claim that the dynamics governing turbulent transport in cold, weakly ionized plasmas look indeed rather different from those from their hotter counterparts. In particular, it is found that turbulent transport behaves in a diffusive manner for timescales beyond the local turbulent timescales, in contrast to the

^{a)}Author to whom correspondence should be addressed. Electronic mail: mierja@unican.es

non-diffusive behavior reported in hotter plasmas. Although these results do not exclude the possibility of observing non-diffusive dynamics in these kind of plasmas, it certainly points to the fact that their relevance may be strongly regime-dependent.

The paper is thus organized as follows: Sec. II presents the experimental setup used for the measurement of the turbulent flux, and gives values for some plasma parameters. In Sec. III, the correlation properties of the measured turbulent fluxes are discussed. In Sec. IV, the flux probability density function (PDF) is first investigated to search for self-similarity, and then from the perspective of the effective phase difference between density and potential fluctuations. The value of this effective phase will prove useful to understand, in particular, the relation between fluctuating turbulent fluxes and the radial shear of the local, mean $\mathbf{E} \times \mathbf{B}$ poloidal flow. Finally, some conclusions are drawn in Sec. VI.

II. EXPERIMENTAL SETUP AND PLASMA PARAMETERS

The plasma inside the Santander Linear Plasma Machine is generated in a cylindrical glass vessel¹⁶ with an internal diameter of 0.07 m and 1 m length (see Fig. 1). The vessel is located inside a circular waveguide 0.08 m in diameter. A magnetized plasma is produced by launching longitudinally electromagnetic waves with a frequency $f = 2.45$ GHz. The vessel has a conical tip facing the microwave generator to reduce the reflected power on the latter. The incident power (P_{LMG}) is in the range $0.6 \text{ kW} < P_{\text{LMG}} < 6 \text{ kW}$ and the system operates in a continuous regime. The stationary longitudinal magnetic field ($0.05 \text{ T} < B < 0.15 \text{ T}$) is generated by six water-cooled coils, which are concentric with the waveguide. All measurements in this work were performed for Helium plasmas with a magnetic field $B = 0.12 \text{ T}$. The mean electron density is determined by using an 8 mm interferometer. An array of Langmuir probes provides the local value of the electron density and floating potential, as long as their fluctuations across the whole plasma radial column. Table I shows typical plasma parameters.

The plasma generated in our machine has cylindrical symmetry so all quantities vary radially. We have examined a great number of flux data obtained by moving the Langmuir probe radially and measuring the flux at ten different, equally spaced radii, from $r = 1 \text{ cm}$ to $r = 2.8 \text{ cm}$ in

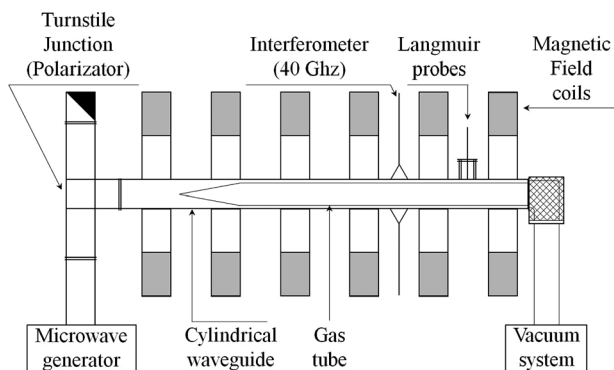


FIG. 1. Scheme of SLPM.

TABLE I. Operating conditions in SLPM.

Parameter	Value
Typical magnetic field (B)	0.12 T
Electron density (n_e)	10^{17} m^{-3}
Electron temperature (T_e)	20 eV
Ion temperature (T_i)	0.05 eV
Debye shielding length (λ_D)	10^{-4} m
Electron Larmor radius (ρ_{Le})	10^{-4} m
Ion Larmor radius (ρ_{Li})	$4 \times 10^{-4} \text{ m}$
Electron cyclotron frequency (f_{ce})	3.4 GHz
Ion cyclotron frequency (f_{ci})	400 kHz
Ionization degree	< 10%

successive shots. No measures have been done further into $r = 1 \text{ cm}$, since the probes themselves and the holder generates great disturbances in the plasma making results unreliable. All previous measures have been performed once the plasma is in a stationary regime.

The array of Langmuir probes consists of four tips, each of tungsten wire 0.5 mm in diameter and 2 mm long. Working on double probe configuration, electron temperature and electron density profiles were obtained. Fluctuations of ion saturation current (\tilde{I}_s) and floating potential ($\tilde{\phi}_f$) were measured using the triple probe configuration, i.e., one probe is in the ion saturation regime while two poloidally separated probes were unbiased to measure the floating potential. Fluctuation measurements were digitized at 1 MHz sampling frequency, 2×10^5 points per channel. All fluctuating quantities are indicated by a tilde and are defined as having zero time-averaged value. The tip on the ion saturation regime located between the other two, but at a slightly displaced radius, it is biased at a fixed voltage to estimate electron density fluctuations. Of course, what the Langmuir probe measures is the ion saturation current, $I_s \propto n\sqrt{T_e}$. Therefore, the flux inferred from these measurements is not necessarily equal to the particle flux. However, measurements of the temperature fluctuations at the plasma edge in some confinement devices such as the TEXT and TJ-I tokamaks, have shown that their relative phase is such that Γ calculated from I_s and ϕ_f is a good estimate of the particle flux.^{17,18} The statistical properties of the radial particle flux, $\Gamma = \tilde{n}\tilde{E}_\theta/B = \tilde{n}(\tilde{\phi}_2 - \tilde{\phi}_1)/(r\epsilon B)$ have been studied from the measured values of the density fluctuations at a given radial position of the plasma, $\tilde{n}(r, \theta, t)$, and the electrostatic plasma fluctuating potential at two nearby positions, $\tilde{\phi}_1(r, \theta - \epsilon/2, t)$ and $\tilde{\phi}_2(r, \theta + \epsilon/2, t)$. Here, r is the radial position of all the probes, θ is the poloidal position of the tip on the ion saturation regime and ϵ is the poloidal displacement between the two poloidally separated probes on the floating potential regime (one is poloidally displaced $-\epsilon/2$ and the other $+\epsilon/2$). Finally, \tilde{E}_θ is the fluctuating poloidal electric field and B the axial magnetic field.

The time evolution of the normalized turbulent radial flux measured at different radial locations across the plasma column is shown in Fig. 2. As in other devices,^{19–21} the flux is predominantly positive (i.e., the particle transport is, on average, outward) and bursty. This temporal behavior of the turbulent particle flux is typical of all measurements carried

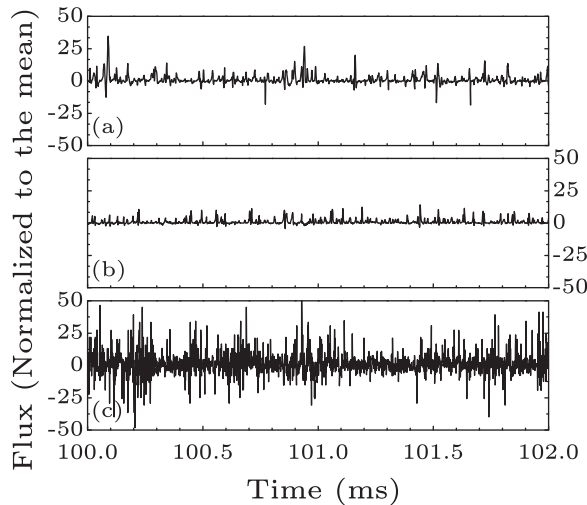


FIG. 2. Time records of the turbulent particle flux in SLPM measured at different radial positions: (a) inner position, $r = 1.0$ cm, (b) intermediate position, $r = 1.8$ cm, and (c) outer position, $r = 2.8$ cm.

out in SLPM. The resulting averaged radial fluxes vary between $10^{18} \text{ m}^{-2}\text{s}^{-1}$ in the outer region and $10^{19} \text{ m}^{-2}\text{s}^{-1}$ in the central region. Although the particle fluxes are quite fluctuating, going in and out of the plasma, the dominant effect is outward because of the averaged (downward) density gradients.

In Fig. 3, the root-mean-square (rms) values of the fluctuating $\mathbf{E} \times \mathbf{B}$ fluxes are drawn at different radial positions, as well as their relative values. The rms values decrease with radius, but a different behavior is observed for the relative rms values, where there is first a decrease in the central part, then a minimum for intermediate positions and finally an increase in the outer region. This can be visually ascertained by looking at Fig. 2, where the normalized fluxes are plotted. In that figure, the normalized fluctuations at intermediate positions (b), are smaller than those for the central and outer regions of the plasma, (a)–(c).

III. CORRELATION PROPERTIES OF THE LOCAL TURBULENT FLUX

A. Autocorrelation

We will discuss first the autocorrelation function of the time series for the fluctuating $\mathbf{E} \times \mathbf{B}$ flux. Results are shown in Fig. 4 for all radial positions. It is apparent that the width of the autocorrelation functions is quite insensitive to the radial position. In addition, the decay appears to be very fast,

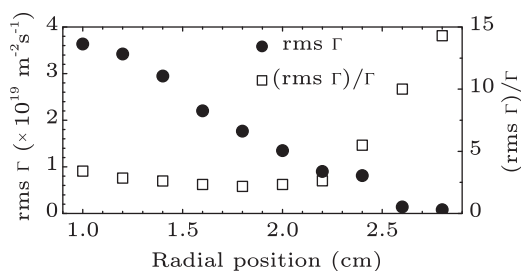


FIG. 3. Rms values (filled circles) and normalized rms values (open squares) of the fluctuating $\mathbf{E} \times \mathbf{B}$ flux in SLPM.

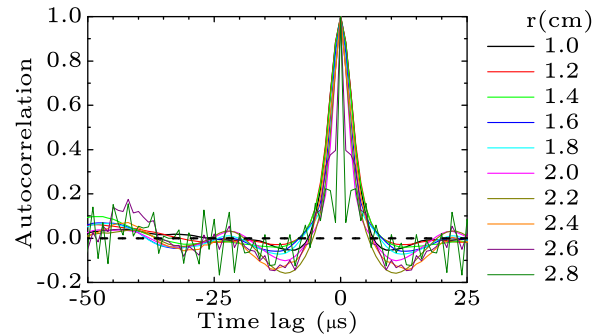


FIG. 4. Autocorrelation functions of the flux series at different radial positions in SLPM.

crossing first through zero for time lags between 6 and 8 μs , which will use as our estimation for the turbulent decorrelation time, τ_d . Long tails appear to be lacking, but it is difficult to see this clearly in the autocorrelation function. It must however be noted that all positions exhibit a bump for time lags in the interval 20–25 μs , followed by a second bump, for twice the time lag values of the first bump, 50–60 μs . This suggests that some periodicity might be present in the time series. We will argue later in the paper that these bumps are consistent with a mean poloidal rotation of the plasma. At the same time, their presence makes our estimate of τ_d somewhat unreliable. We will discuss a second, better estimate in Sec. III B.

B. Hurst exponent

In order to clarify whether long-term correlation (i.e., long tails) are present or not in the data, we have also performed the R/S statistics proposed by Mandelbrot and Wallis,²² based on the previous work of Hurst.²³ This analysis is carried out in the following way. Let us suppose we have a temporal signal $s(t)$. First, the mean of the signal is subtracted, $\hat{s}(t) = s(t) - \bar{s}$. Then, we assume that $\hat{s}(t)$ provides the increments of a random walk after a lapse of time τ . The distance traveled by the walker is, at time t , given by $S(\tau) = \int^\tau \hat{s}(t') dt'$. Then, we define the range of the motion as the difference between the maximum and minimum of S . Finally, this range is rescaled by the standard deviation of the data, so the quantity R/S is the rescaled range. The results are then interpreted as follows. If the sequence has short-range correlations (i.e., correlations up to a temporal range $\tau \lesssim \tau_d$, where τ_d is the decorrelation time of the signal), the expected value of $R(\tau)/S(\tau)$ scales as $\tau^{1/2}$ for time lags $\tau > \tau_d$. On the other hand, if long-range correlations are present, the expected value of $R(\tau)/S(\tau)$ scales as τ^H with $H \neq 1/2$ for $\tau \gg \tau_d$. These correlations are positive (i.e., persistence) if $1 > H > 0.5$. For $0.5 > H > 0$ correlations are negative (anti-persistence).

Fig. 5(a) shows the results for the R/S analysis carried out at different radial locations in SLPM. In all cases, a region with $H \sim 1/2$ beyond $\tau_r \sim 30 \mu\text{s}$ is found (region to the right of the vertical, dashed line in figure), that extends up to the longest times available. To help to guide the eye, two oblique lines have been included in the figure that represent the theoretical curves for two different dynamical behaviors,

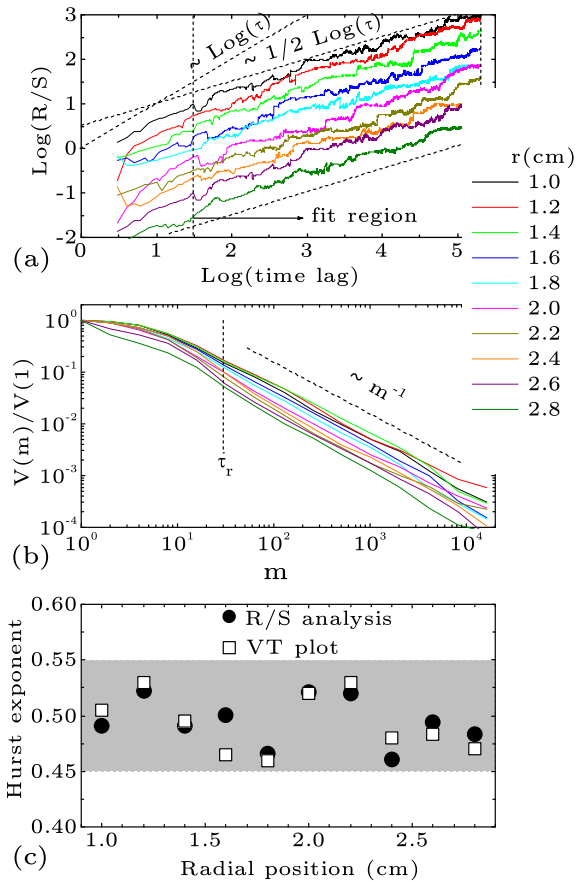


FIG. 5. (a) R/S analysis of the flux series at different radial positions in SLPM. The curves have been shifted down successively to better appreciate long-range time dependencies. (b) Variance for each of the series $\Gamma^{(m)}$ derived from the original measured flux series at different radii, as a function of m . (c) Hurst exponents obtained from the linear fits of the graphs shown in (a) (R/S analysis, filled circles) together with those obtained from the linear fits of the graphs shown in (b) (VT analysis, hollow squares).

namely, a deterministic process in which $R/S \sim \tau$ (dashed line) and a random, Gaussian process in which $R/S \sim \tau^{1/2}$ (dotted line). To quantify the behavior, power-law fits have been made for the time interval ranging from 30 to 200 000 μs . Fig. 5(c) (filled circles) shows the exponents obtained. In all cases, the values for H fall within the interval $[0.46, 0.52]$ (the shaded region represents the symmetric interval $[0.45, 0.55]$ around $H = 1/2$).

Finally, we note that the transition time-lag between correlated and random regions, $\tau_d \sim 20\text{--}30 \mu\text{s}$, is probably a better estimate of what the local decorrelation time is than that provide by the first zero-crossing of the auto-correlation function in the presence of periodicities.

C. Variance-time plot

To confirm the goodness of the Hurst exponents obtained with the R/S analysis, we have recalculated them using the Variance-Time (VT) plot analysis.²⁴ This method is based on the slowly decaying variance property of any process undergoing aggregation. Considering any time record $X \equiv \{X_j; j = 1, 2, \dots, N\}$, being X_j the value for the variable X at time j , and N the total number of temporal points, the

m -averaged process, $X^{(m)} = \{X_j^{(m)}; j = 1, \dots, N/m\}$, of the original discrete time parent process X is defined as

$$X_j^{(m)} = \frac{1}{m} \sum_{i=(j-1)m+1}^{jm} X_i, \quad j = 1, 2, \dots, N/m, \quad (1)$$

where m and j are positive integers. The averages are performed over non-overlapping temporal windows containing m elements from the original measured time series. As stated above, $X^{(m)}$ is the resulting temporal averaged series coming from the original signal X or in other words, is the original record with a degraded resolution by a factor m , where m is increased by powers of 2 ($m = 2^1, 2^2, \dots, 2^{14} = m_{\text{max}} = 16384$). The variance is defined as

$$\text{Var}[X^{(m)}] = \frac{1}{N/m} \sum_{j=1}^{N/m} (X_j^{(m)} - \bar{X})^2. \quad (2)$$

The variances of the aggregated processes $X^{(m)}$ decrease with m (for large m)

$$\text{Var}[X^{(m)}] = \text{Var}[X]/m^\beta, \quad (3)$$

where $\beta = 2(H-1)$, being H the self-similarity parameter or Hurst exponent.

The VT plot is obtained by plotting $\log(\text{Var}[X^{(m)}])$ against $\log(m)$ and by fitting a least-square line through the resulting points ignoring those for small values of m . For most processes, the value of β is -1 , indicating that no self-similar behavior occurs (i.e., stochastic processes). On the other hand, when the points are aligned in a line which is flatter than that ($0 < \beta < -1$), the process has features of self-similarity, and an estimate for the degree of self-similarity is given by $H = 1 + \beta/2$. According to Eq. (3), the self-similarity ranges are the regions in m where the condition $\text{Var}[X^{(m)}] \propto m^\beta \equiv m^{2(H-1)}$ is fulfilled and $\beta \neq -1$ ($H \neq 1/2$).

In Fig. 5(b), the resulting variances, $\text{Var}[\Gamma^{(m)}]$, for each averaged $\Gamma^{(m)}$ have been plotted. We have divided the temporal scales in two different ranges: the fluctuation range, comprising the interval $t \leq \tau_r \sim 30 \mu\text{s}$, and the long temporal scale range, in the interval $t \geq \tau_r \sim 30 \mu\text{s}$, being τ_r a limiting temporal scale between these two temporal ranges.

For temporal scales longer than τ_r ($m \geq 32$), the system behaves stochastically since $\beta \sim -1$ is obtained for all radii and hence $H \sim 1/2$. Fig. 5(c) (hollow squares) shows the detailed results, together with those obtained using the R/S analysis to highlight the agreement.

D. Power spectra

Another popular method to look for correlations in time series is the investigation of their power spectra. Here, flat regions are usually associated to random dynamics, whilst f^{-s} regions, with $0 < s < 1$ are attributed to the existence of long-term memory and correlations. The power spectrum of the turbulent fluxes at different positions is shown in Fig. 6(a). It shows different scaling behaviors as we move in the radial direction. For the two innermost positions, there are

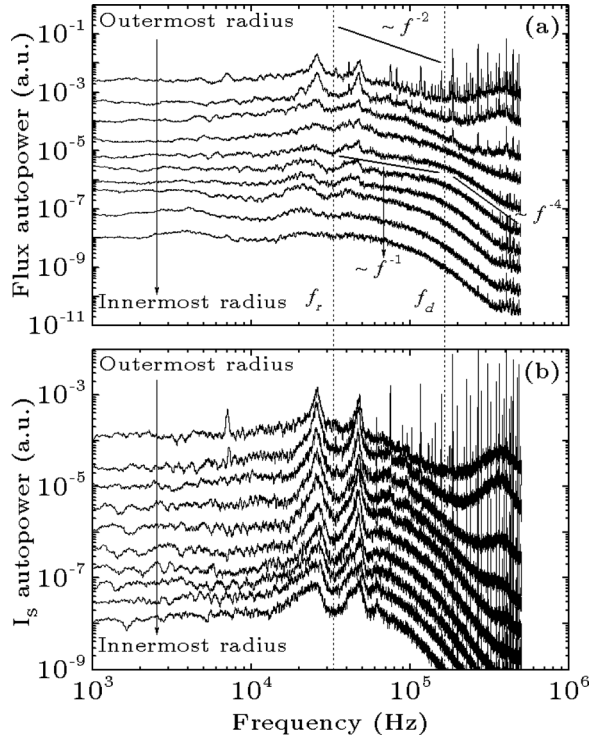


FIG. 6. Power spectra of: (a) particle flux time series and (b) ion saturation current time series at different radial positions.

three distinct regions in the power spectra. For the highest frequencies ($f > f_d = 1/\tau_d \sim 1.7 \times 10^5$ Hz, where τ_d is the flux decorrelation time introduced earlier and f_d is represented graphically by the right dashed-vertical line), the data show a scaling behavior close to f^{-4} . For the lowest frequencies ($f < f_r = 1/\tau_r \sim 3.3 \times 10^4$ Hz, where f_r is represented by the left dashed-vertical line), the data show a nearly flat behavior. For frequencies in between ($f_r < f < f_d$), no clear algebraic trend can be identified. In fact, the trend seems to be exponential. For the four outermost positions, there are two distinct regions in the power spectra: For frequencies in the range $f > f_r$, the data show a scaling behavior of approximately f^{-2} . At lower frequencies, $f < f_r$, the data show a nearly flat trend. Finally, for the remaining four intermediate positions, there appears to be three distinct regions in the power spectra: For the lowest ($f < f_r$) and highest ($f > f_d$) frequencies, the scaling is similar to that for the two innermost radial locations, but for intermediate frequencies ($f_r < f < f_d$) the spectral decay is closer to f^{-1} . This exponent has often been associated to self-organized-critical dynamics.^{25,26} However, the fact that an associated region is absent in the R/S analysis suggests that it might also be just a transition region with no dynamical meaning. A very robust feature in all the spectra in Fig. 6(a) that is worth discussing is the fact that all of them exhibit two peaks at frequencies $f_1 \sim 25 \times 10^3$ Hz and $f_2 \sim 48 \times 10^3$ Hz, respectively. These peaks, which are much more apparent when visualizing the power spectra of the ion saturation current (i.e., the fluctuating density) time series [see Fig. 6(b)], are consistent with the expected frequency of the mean $\mathbf{E} \times \mathbf{B}$ drift, with velocity $\mathbf{v} = \mathbf{E} \times \mathbf{B}/B^2$. Typical values for the mean radial electric field in SLPM are around 400–500 V/m, being approximately

uniform in the radial interval between the innermost and outermost radial positions, $r_i = 1.0$ cm and $r_o = 2.8$ cm, respectively. The magnetic field is uniform, being its value $B = 0.12$ T. Thus, the associated drift frequencies, f_d , should fall within the interval $[f_o, f_i] \simeq 20, 60 \times 10^3$ Hz, which is in agreement with the values obtained by inspecting the peaks in Fig. 6. This radially sheared, poloidal $\mathbf{E} \times \mathbf{B}$ drift could be responsible of the decorrelation of the turbulence on temporal scales above $\tau_r \sim f_r^{-1}$, consistent with the value of the Hurst exponent found there, $H \sim 1/2$, in all radial locations.

IV. INVESTIGATION OF THE PDF OF THE LOCAL TURBULENT FLUXES

A. Self-similarity

After examination of correlation properties, we proceed now to look at the statistics for the sake of completeness. We start by looking for self-similar properties of the PDF of the turbulent fluxes at different radial locations. We have calculated these PDFs over different time resolutions by using Eq. (1). $m=1$ gives the original series, whilst the m -averaged fluxes, $\Gamma_t^{(m)}$ have been computed by averaging over blocks of size 2^m , $m = 1, 2, \dots, 11$. Each reduction in resolution implies a decrement in the statistics. This limits the largest exponent to $m=11$ (i.e., 2048 elements), since $\Gamma_t^{(m)}$ then consists of only $N/m = 200\,000/2048 < 100$ points. To different scalings are then observed depending on the value of m . For $m < 16$, we encounter the fluctuation range, with times up to the order of τ_d . The rescaled flux PDFs are shown in Fig. 7(a) for the radial location $r = 1.6$ cm. The rescaling exponent that makes the PDFs collapse has been found to be $H \sim 0.75$, consistent with the correlated behavior within the central region of the autocorrelation function of the flux.

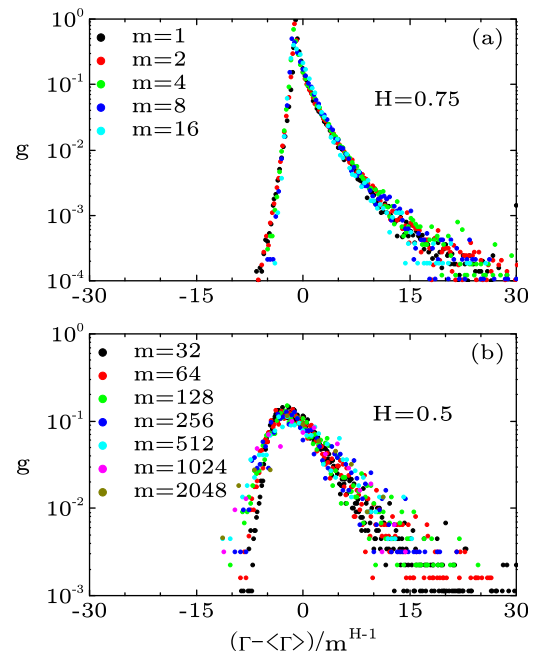


FIG. 7. (a) Rescaled PDFs of the local turbulent fluxes at $r = 1.6$ cm for $m < 16$ and scaling parameter $H = 0.5$. (b) Rescaled PDFs for $m > 16$ and $H = 0.5$ at the same location.

For $m > 16$, the shape of the rescaled PDFs changes. The results are shown in Fig. 7(b). The best collapse is found by choosing the rescaling exponent $H \sim 0.5$, although there is significant deviation at the end of the positive tail. This exponent is consistent with the value of the Hurst exponent found from the R/S analysis over this range of scales.

V. EFFECTIVE PHASE-DIFFERENCE ANALYSIS

The PDFs of the local fluxes measured in SLPM are clearly non-Gaussian for any radial position as seen in Fig. 7. Nonetheless, the fluctuating quantities from which the fluxes are calculated, density and potential, follow near-Gaussian statistics. Fig. 8 shows the PDFs of the measured fluctuating potential (a)–(b) and ion saturation current (c)–(d) at different radial positions. For every radius, the PDFs of the potential fluctuations are near-Gaussian, while for the ion saturation current (related to the density) the PDFs are near-Gaussian for negative values but seem to develop a slightly more exponential character when the argument takes positive values.

It is possible to infer the expected PDF of the fluctuating fluxes by assuming that a certain effective phase difference exists between density and potential fluctuations.¹ Indeed, fluctuating fluxes are obtained from the product of density and radial velocity fluctuations, $\Gamma = \tilde{n}\tilde{V}_r$, which in turn are estimated from the experimental measurements obtained with Langmuir probes for both the plasma ion saturation current and floating potential. The ion saturation current is not strictly Gaussian, as can be seen in Figs. 8(c) and 8(d), but it can be considered that Gaussian behavior is a good approximation. Thus, the fluctuating density, which is in turn calculated assuming $\tilde{n} \propto \tilde{I}_s$, is also Gaussian. On the other hand, since the electrostatic potential fluctuation, $\tilde{\phi}$, is Gaussian, its derivative with respect to the poloidal angle, $\tilde{V}_r = (1/rB)(\partial\tilde{\phi}/\partial\theta)$, must also be Gaussian. Assuming an effective correlation γ ($-1 \leq \gamma \leq 1$), between density and

potential fluctuations, the PDF of their product can be obtained to be¹

$$p(\Gamma) = \frac{1}{\pi\sqrt{1-\gamma^2}\langle\tilde{n}^2\rangle^{1/2}\langle\tilde{V}_r^2\rangle^{1/2}} \times K_0\left(\frac{|\Gamma|}{(1-\gamma^2)\langle\tilde{n}^2\rangle^{1/2}\langle\tilde{V}_r^2\rangle^{1/2}}\right) \times \exp\left(-\gamma\frac{\Gamma}{(1-\gamma^2)\langle\tilde{n}^2\rangle^{1/2}\langle\tilde{V}_r^2\rangle^{1/2}}\right), \quad (4)$$

where γ measures the strength and the sign of the correlation between \tilde{n} and \tilde{V}_r . The mean squared values, $\langle\tilde{n}^2\rangle$ and $\langle\tilde{V}_r^2\rangle$, are the variances of \tilde{n} and \tilde{V}_r . The K_0 is the modified Bessel function of the second kind and order zero.

From Eq. (4), the mean value of the product Γ is

$$\langle\Gamma\rangle = \langle\tilde{n}\tilde{V}_r\rangle = -\gamma\langle\tilde{n}^2\rangle^{1/2}\langle\tilde{V}_r^2\rangle^{1/2}. \quad (5)$$

From Eq. (5), we get that for the averaged flux to be outward, null or inward, γ must, respectively, be negative, zero, or positive. Moreover, we can obtain experimentally the correlation between fluctuating density and fluctuating radial velocity just by dividing the mean flux by the product of the density and radial velocity standard deviations. Another method to obtain γ is by fitting the experimental flux PDFs against the analytical PDF, Eq. (4). In Fig. 9, we have plotted the flux PDF obtained from the experiment at radial position $r = 1.6$ cm, together with three analytical PDFs given by Eq. (4) for different values of the parameter γ . It is apparent that this functional form well describes practically the entire experimental PDF, except perhaps the very large $|\Gamma|$ tails.

The shape of the local flux PDF present a systematic variation as a function of the radial position, which implies a change in the relative phase between density and radial velocity fluctuations as we move in the radial direction. To see this effect, in Fig. 10 we have plotted the radial dependence of γ as obtained from the two methods previously described. The results obtained using both techniques are in agreement: there is an initial increase of the correlation as we probe

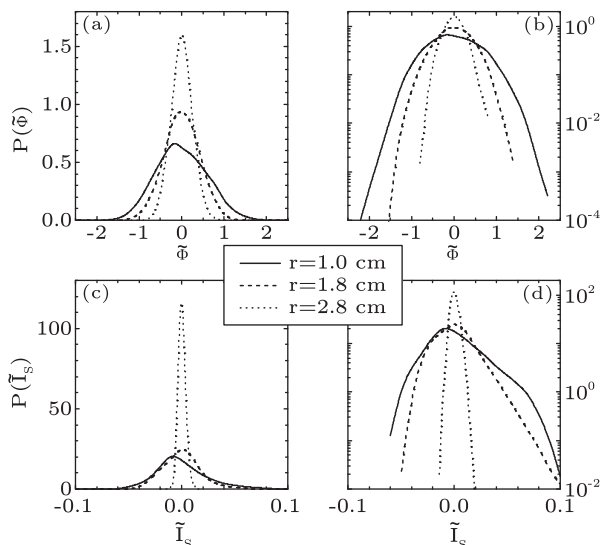


FIG. 8. Probability distribution functions of: (a) $\tilde{\phi}$ in lin-lin scale, (b) $\tilde{\phi}$ in log-lin scale, (c) \tilde{I}_s in lin-lin scale, and (d) \tilde{I}_s in log-lin scale, at three different radial locations.

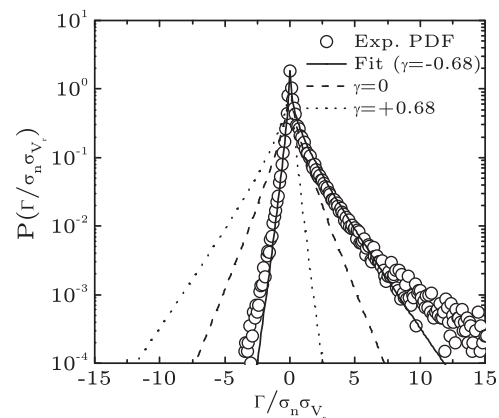


FIG. 9. Comparison of the experimental flux PDF at $r = 1.6$ cm (open circles) with three analytical PDFs calculated from Eq. (4). The full line corresponds to the best fit ($\gamma = -0.68$), the dashed line corresponds to $\gamma = 0$ and the dotted line corresponds to $\gamma = +0.68$.

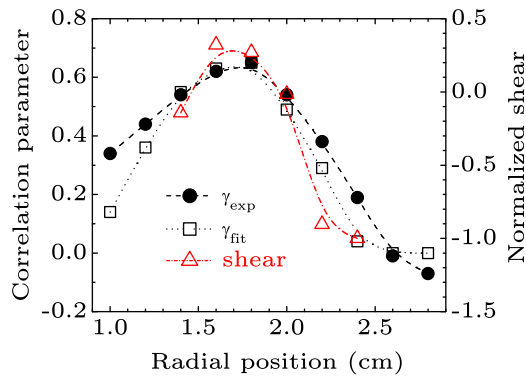


FIG. 10. Radial dependence of the correlation parameter γ between density and radial velocity fluctuations (open squares and filled circles), calculated in two different ways (see text). Triangles stand for the mean local value of the shear of the poloidal angular velocity.

increasing radial positions, reaching a maximum around $r = 1.8$ cm, and decreasing for the outermost positions.

To try to understand the origin of this variation, we have also computed the mean local value of the shear of the angular velocity associated to the poloidal $\mathbf{E} \times \mathbf{B}$ flow, that can be obtained from the experimental values of the averaged floating potential. The results are shown in Fig. 10 using triangles. Values have been obtained only for the six central positions since the numerical value of the shear at r_i depends on the value of the electric potential at positions r_{i-2} , r_{i-1} , r_i , r_{i+1} and r_{i+2} . From the figure, it is clear that the radial locations where the correlation is higher correspond to the regions where the shear of the poloidal flow is smaller. On the contrary, in regions where the value of the shear is larger, the correlation is smaller. But even in those regions where the shear is weaker and the correlation larger, the R/S analysis suggests that the dynamics are not capable of establishing the kind of long-term correlations that may yield non-diffusive transport features.

VI. CONCLUSIONS

In this work, we have quantified the statistical and correlation properties of the fluctuating turbulent fluxes measured by means of a movable array of Langmuir probes in cold, weakly ionized helium plasmas inside the Santander Linear Plasma Machine. These studies have been carried out to help to determine whether the dynamics of transport in these plasmas should be expected to be similar to those characteristic of the much hotter, ionized plasmas confined in tokamaks or stellarators. For that reason, we have used the same techniques employed to characterize tokamak/stellarator data in the past. The results of the analysis suggest that the dynamics of transport in colder, weakly ionized plasmas are indeed quite different. No long-term correlations whatsoever seem to be present in the data, except at the shortest timescales associated to the central part of the autocorrelation function of the flux (where some non-Gaussianity, specially in the saturation current fluctuations is apparent). For larger timescales, all methods of analysis used here suggest that randomness dominates the dynamics (i.e., Hurst exponents $H \sim 1/2$), which is consistent with radial turbulent transport exhibiting a rather diffusive nature.

We have also quantified the correlation between the density and potential fluctuations at different locations. We have found that this correlation is largest at the locations where the radial shear in the poloidal angular velocity (associated to the dominant mean $\mathbf{E} \times \mathbf{B}$ flow) is weaker. But even at the locations where the shear is weaker and the correlation strongest, the dynamics do not seem to be capable of establishing the kind of long-term correlations that we see in hotter tokamak/stellarator plasmas.

These results and conclusions are consistent with past theoretical studies carried out in the context of a diffusive running sandpile as a paradigm for a confined plasma^{25,26} and with numerical simulations of drift wave turbulence in near-marginal conditions.^{27,28} These studies showed that the presence of any memory-erasing mechanism that competes with turbulent transport could, even when close near-marginal conditions, impede the establishment of any long-term correlation even at subdominant strengths. It is not clear whether the cold, weakly ionized plasmas inside SLM are close to marginality or not. But even if they were, the large collisional diffusion present at temperatures of a few eVs could play the role of a memory-erasing mechanism. Another possible candidate could also be the losses caused by free-streaming along the open field lines in the linear device. Either way, the final result would be a system where turbulent transport would behave rather diffusively. In contrast, the closed field lines and the very low diffusivities typical of hot tokamak/stellarator plasmas could open the possibility for the observation of different transport dynamics. Of course, our results do not exclude the possibility that a cold plasma may exhibit non-diffusive dynamics, if it could be brought into a regime in which near-marginal conditions may be achieved. But they certainly suggest that their dynamics are not universal, but regime-dependent.

ACKNOWLEDGMENTS

This research was sponsored by DGICYT (Dirección General de Investigaciones Científicas y Tecnológicas) of Spain under Projects MICINN ENE2009-12213-C03-03 and MINECO ENE2012-33219. Research supported in part by DOE Office of Science Grant No. DE-FG02-04ER5741 at University of Alaska.

¹B. A. Carreras, C. Hidalgo, E. Sánchez, M. A. Pedrosa, R. Balbín, I. García-Cortés, B. van Milligen, D. E. Newman, and V. E. Lynch, *Phys. Plasmas* **3**, 2664 (1996).

²A. J. Wootton, B. A. Carreras, H. Matsumoto, K. McGuire, W. A. Peebles, Ch. P. Ritz, P. W. Terry, and S. J. Zweben, *Phys. Fluids B* **2**, 2879 (1990).

³Ch. P. Ritz, R. V. Bravenec, P. M. Schoch, R. D. Bengtson, J. A. Boedo, J. C. Forster, K. W. Gentle, Y. He, R. L. Hickok, Y. J. Kim, H. Lin, P. E. Phillips, T. L. Rhodes, W. L. Rowan, P. M. Valanju, and A. J. Wootton, *Phys. Rev. Lett.* **62**, 1844 (1989).

⁴B. A. Carreras, B. van Milligen, C. Hidalgo, R. Balbin, E. Sanchez, I. Garcia-Cortes, M. A. Pedrosa, J. Bluel, and M. Endler, *Phys. Rev. Lett.* **83**, 3653 (1999).

⁵B. A. Carreras, B. Ph. van Milligen, M. A. Pedrosa, R. Balbin, C. Hidalgo, D. E. Newman, E. Sanchez, M. Frances, I. García-Cortés, J. Bleuel, M. Endler, S. Davies, and G. F. Matthews, *Phys. Rev. Lett.* **80**, 4438 (1998).

⁶T. L. Rhodes, R. A. Moyer, R. Groebner, E. J. Doyle, R. Lehmer, W. A. Peebles, and C. L. Rettig, *Phys. Lett. A* **253**, 181 (1999).

- ⁷B. A. Carreras, V. E. Lynch, D. E. Newman, R. Balbín, J. Bleuel, M. A. Pedrosa, M. Endler, B. Ph. van Milligen, E. Sánchez, and C. Hidalgo, *Phys. Plasmas* **7**, 3278 (2000).
- ⁸R. Sánchez, B. Ph. van Milligen, D. E. Newman, and B. A. Carreras, *Phys. Rev. Lett.* **90**, 185005 (2003).
- ⁹Y. H. Xu, S. Jachmich, R. R. Weynants, A. Huber, B. Unterberg, and U. Samm, *Phys. Plasmas* **11**, 5413 (2004).
- ¹⁰V. P. Budaev, S. Savin, L. Zelenyi, N. Ohno, S. Takamura, and E. Amata, *Plasma Phys. Controlled Fusion* **50**, 074014 (2008).
- ¹¹V. P. Budaev, S. Takamura, N. Ohno, and S. Masuzaki, *Nucl. Fusion* **46**, S181–S191 (2006).
- ¹²G. Y. Antar, S. I. Krashennnikov, P. Devynck, R. P. Doerner, E. M. Hollmann, J. A. Boedo, S. C. Luckhardt, and R. W. Conn, *Phys. Rev. Lett.* **87**, 065001 (2001).
- ¹³J. E. Maggs and G. J. Morales, *Phys. Rev. Lett.* **107**, 185003 (2011).
- ¹⁴G. Hornung, B. Nold, J. E. Maggs, G. J. Morales, M. Ramisch, and U. Stroth, *Phys. Plasmas* **18**, 082303 (2011).
- ¹⁵B. Ph. van Milligen, R. Sánchez, and C. Hidalgo, *Phys. Rev. Lett.* **109**, 105001 (2012).
- ¹⁶O. F. Castellanos, E. Anabitarte, J. M. Senties, C. Hidalgo, and M. A. Pedrosa, *Plasma Phys. Controlled Fusion* **47**, 2067 (2005).
- ¹⁷H. Lin, R. D. Bengtson, and Ch. P. Ritz, *Phys. Fluids B* **1**, 2027 (1989).
- ¹⁸C. Hidalgo, R. Balbín, M. A. Pedrosa, I. García-Cortés, and M. A. Ochando, *Phys. Rev. Lett.* **69**, 1205 (1992).
- ¹⁹C. Hidalgo, *Plasma Phys. Controlled Fusion* **37**, A53 (1995).
- ²⁰M. Endler, H. Niedermeyer, L. Giannone, E. Holzhauser, A. Rudyj, G. Theimer, N. Tsois, and ASDEX Team, *Nucl. Fusion* **35**, 1307 (1995).
- ²¹T. Huld, A. H. Nielsen, H. L. Pécseli, and J. J. Rasmussen, *Phys. Fluids B* **3**, 1609 (1991).
- ²²B. B. Mandelbrot and J. R. Wallis, *Water Resour. Res.* **5**, 967, doi:10.1029/WR005i005p00967 (1969).
- ²³H. E. Hurst, *Trans. Am. Soc. Civ. Eng.* **116**, 770 (1951).
- ²⁴H. F. Zhang, Y. T. Shu, and O. Yang, in *Proceedings of the IEEE Pacific Rim Conference on Communications, Computers and Signal Processing, Victoria BC, 1997*, Vol. 2, pp. 883–886.
- ²⁵D. E. Newman, B. A. Carreras, P. H. Diamond, and T. S. Hahm, *Phys. Plasmas* **3**, 1858 (1996).
- ²⁶R. Sánchez, D. E. Newman, and B. A. Carreras, *Nucl. Fusion* **41**, 247 (2001).
- ²⁷J. A. Mier, L. García, and R. Sánchez, *Phys. Plasmas* **13**, 102308 (2006).
- ²⁸J. A. Mier, R. Sánchez, L. García, D. E. Newman, and B. A. Carreras, *Phys. Plasmas* **15**, 112301 (2008).